Applied Thermal Engineering 178 (2020) 115580

Contents lists available at ScienceDirect

Applied Thermal Engineering

journal homepage: www.elsevier.com/locate/apthermeng

Detailed experimental analysis of the energy performance of a desiccant wheel activated at low temperature

F. Comino*, F. Táboas, F. Peci, M. Ruiz de Adana

Departamento de Química-Física y Termodinámica Aplicada, Escuela Politécnica Superior, Universidad de Córdoba, Campus de Rabanales, Antigua Carretera Nacional IV, km 396, 14071 Córdoba, Spain

HIGHLIGHTS

- The performance of the DW varied along the heat and mass transfer surface.
- Desiccant surface temperatures varied for different rotation speeds.
- The highest efficiencies of the DW were obtained in the last circular sector.
- The MRC value can be controlled by varying rotation speeds and air flow rates.

ARTICLE INFO

Keywords:
Desiccant wheel performance
Regeneration efficiency
Desiccant material temperature
Low temperature activated systems

ABSTRACT

Desiccant dehumidification systems, such as those using desiccant wheels (DW), are an interesting alternative to conventional dehumidification systems based on vapor-compression cycles. The aim of this work was to obtain experimentally the performance of a DW activated at low temperature along the heat and mass transfer surface under different working conditions. The air temperature and humidity were measured at 32 different points, in order to analyse the performance of the DW at different circular sectors of the rotor.

The results showed that the surface temperatures of the desiccant material on the process side decreased when the rotation speed decreased. Conversely, the surface temperatures of the desiccant material on the regeneration side increased when the rotation speed decreased.

The minimum outlet process air temperatures and the maximum process air dehumidification were obtained in the circular sector closest to the regeneration side. In this circular sector the highest efficiency values were obtained. The number of circular sectors where the highest efficiency values were obtained increased when the rotation speed or air flow rates increased. Using these data, the wheel control strategy could be designed to increase the dehumidification capacity.

1. Introduction

Conventional heating, ventilation and air conditioning (HVAC) systems are responsible for a significant percentage of the EU energy consumption [1]. Managing air with an efficient HVAC system, which does not depend mainly on electrical energy and does not use any refrigerant, could be an interesting alternative to conventional HVAC systems based on vapor-compression cycles. Desiccant dehumidification systems, such as a desiccant wheel (DW) present a promising alternative to conventional dehumidification units.

A DW typically rotates slowly, exchanging heat and moisture between the process air stream and the regeneration air stream. The most influential parameter affecting the desiccant capacity of a DW is the regeneration air temperature [2]. Usually, a DW is thermally activated at high temperatures, although previous research showed acceptable desiccant capacity when regeneration temperatures were below 60 °C [2,3]. In addition, the use of low regeneration air temperatures easily allows the combination of a DW with other HVAC elements, such as an indirect evaporative cooling system [4–7] or a heat pump [8], renewable energy sources, such as solar thermal energy [9,10], or waste heat systems [11]. The outlet process air temperature rise is directly proportional to the amount of moisture removed from the inlet process air flow [12]. Therefore, it is necessary to properly control both outlet air temperature and humidity ratio of a DW activated at low temperature.

A widely used method to analyse DW behaviour is through mathematical models [13]. Several authors have developed mathematical

* Corresponding author.
E-mail address: francisco.comino@uco.es (F. Comino).

https://doi.org/10.1016/j.applthermaleng.2020.115580
Received 2 March 2020; Received in revised form 27 May 2020; Accepted 7 June 2020
Available online 10 June 2020
1359-4311/

Nomenclature

1p-8p; 1r-8r	air states
h	enthalpy [kJ kg^{-1}]
MRC	moisture removal capacity [kg h^{-1}]
$\dot{m}$	mass air flow rate [kg h^{-1}]
N1-N24	experimental tests
P	pressure [Pa]
R	rotation speed [rph]
RH	relative humidity
T	temperature [°C]
$\dot{V}$	volumetric air flow rate [m^3 h^{-1}]

Greek letters

Δ	increment, decrement
ε	regeneration efficiency
ρ	density [kg m^{-3}]
ω	humidity ratio [g kg^{-1}]

Subscripts

HC	heating coil
i	inlet
o	outlet
p	process
r	regeneration
vap	vaporisation of water

Superscripts

–	average value

Acronyms

AHU	air handling unit
DW	desiccant wheel
EA	exhaust air
F	centrifugal fan
FC	flow conditioner
HVAC	heating, ventilating and air conditioning
NTC	negative temperature coefficient
OA	outdoor air
PT	pitot tube

models to analyse heat and mass transfer in a DW, that mainly depend on the adsorbent material of the rotor and its working conditions [14]. A mathematical model of a DW using heat and mass transfer partial differential equations was obtained in [15]. This model provided equations similar to those of a rotary heat exchanger and, they were described by the Effectiveness-NTU method. A one-dimensional gas side resistance DW model that solves heat and mass transfer equations was developed in [16]. In this paper, the authors identified the most efficient circular sector of the process air using this mathematical model. Other authors also obtained gas side resistance based fully explicit algebraic expressions taking into account the split ratio of a DW [17]. These authors also modelled the heat and mass transfer in a DW into a set of linear differential equations, under the linearization assumptions on the temperature and humidity profiles and the psychrometric relationship [18]. In this study, it was found that the behaviour of a DW depends on the sorption capacity and transfer capacity of the DW and the psychrometric relation of the air. In another research study, the adsorption and desorption capacity of a DW were also analysed using a transient one-dimensional mathematical model [19]. This model was mainly used to obtain the optimum rotation speed for different case studies. A one-dimensional coupled heat and mass transfer DW model was developed in other studies, taking into account the dependence of thermodynamic and transport properties of humid air with temperature [20]. This model was analysed in terms of outlet process air temperature and humidity profiles, dehumidification effectiveness and sensible energy ratio. However, these mathematical models were developed by measuring outlet air conditions at a single point, mixed outlet air conditions, without taking into account the heat and mass transfer in each circular sector of the wheel.

Some researchers developed DW mathematical models measuring the outlet air conditions in different circular sector. A DW model based on the dehumidification capacity prediction was obtained using transient measurements of a real installation [21]. The experimental transient measurements were obtained with an interesting system that measured outlet air conditions from different directions. Another DW model was developed and validated in [22], in order to analyse the effects of the regeneration air temperature, air superficial velocity, wheel thickness and wheel rotational speed. In this work, the temperature and dew-point temperature distributions of the process air in the wheel circumferential and radius directions at the process air outlet were also measured. The experimental measures taken in these works were used to ensure the mixed air conditions, obtaining average values of outlet process air temperature and humidity ratio.

Other authors experimentally analysed performance of a DW as a function of heat and mass transfer [23]. Desiccant capacity and sorption performance for different DWs and different rotation speeds were obtained experimentally in [24] and an optimum rotation speed was obtained for each type of wheel. An experimental study comparing the dehumidification performance of different adsorbent materials for a DW was carried out in [25]. The results provided some insights and guidelines for the design and optimization of a DW. The heat and mass transfer of a DW made of a polymeric desiccant were investigated at a low regeneration temperature in order to use low thermal energy grade [26]. In this case, the dehumidification performance was determined for several air velocities and rotational speeds. Another experimental study also obtained the dehumidification performance of DW manufactured with silica-based adsorbents [27]. The static and dynamic sorption characteristics were directly measured by a gravimetric method, which measured the changes in the weight of the DW during the adsorption and desorption processes. These experimental studies of DW performance were carried out without taking into account the effects of heat and mass transfer that exist in each sector of the rotor.

Based on the need to accurately adjust the outlet process air temperature and humidity ratio of a DW activated at low temperature, a detailed analysis of the DW performance measured at different areas of the heat and mass transfer surface of the rotor could be carried out. This analysis has not been studied in detail in the existing literature when a DW activated at low temperature was operational, neither in mathematical models, nor in experimental transient studies or experimental parametric studies. Therefore, the main objective of this work was to obtain experimentally the performance of a desiccant wheel activated at low temperatures along the heat and mass transfer surface under different working conditions. To achieve this, the air temperature and humidity were measured at 32 different points, in order to analyse the performance of different circular sectors of the DW. Experimental results could also be very useful for modelling desiccant dehumidification systems, since most experimental works measured the inlet and outlet air conditions at a single point.

2. Methodology

2.1. Experimental setup

The performance of a DW activated at low temperatures was analysed experimentally. An experimental test facility was used to study the DW, as shown in Fig. 1. This test facility provided two air flows to simulate different air conditions. Two air handling units (AHU) were used to adjust setpoint conditions: air temperature and humidity ratio in the inlet airflow to the DW. Each AHU was composed of a heating coil, a cooling coil, an electric heater and a steam humidifier. Four centrifugal fans of variable speed were used to adjust the process and regeneration air flow rates. Moreover, two flow conditioners in each air stream enabled stable air flow conditions to be obtained. A detailed description of the test facility and the technical characteristics of the HVAC elements was included in a previous study [28]. The analysed DW was composed of alternate layers of flat and corrugated sheets of silica gel and metal silicates. The technical characteristics and nominal conditions of the DW are shown in Table 1.

The inlet and outlet air conditions of the two air streams of the DW were measured at different positions of the rotor. A thin grid with eight sensors of air temperature and humidity was installed at each side of the wheel, with a total of 32 sensors. The distribution of the grids and sensors is shown in Fig. 2. The sensors on the input process side and input regeneration side were installed in order to check that the experimental conditions were uniform and steady-state. The sampling time was 3 s and the values measured with each sensor were averaged every 20 min.

Air temperature, T, was measured using NTC (negative temperature coefficient) sensors, with an accuracy of ± 0.2 °C, at each acquisition point, as shown in Fig. 2. Air relative humidity, RH, was measured using capacitive sensors, with an accuracy of ± 2%, at each acquisition point, as shown in Fig. 2. Differential pressure, ΔP, was measured to obtain the process and regeneration air flow rates, V̇, with a differential pressure transmitter, with an accuracy of ± 0.3%, see Fig. 1. A thermographic camera was used to obtain thermal images of the desiccant material.

Table 1
Technical characteristics of the desiccant wheel.

Parameter	Value
Nominal capacity	15 [kg/h] [a)]
Nominal air flow rate	2300 [m^3/h] [b)]
Rotor diameter	550 [mm]
Rotor thickness	200 [mm]
Nominal rotation	40 [rph]
Regeneration circular sector	180 [°C]
Desiccant material	Silica gel
Silica gel density	800 [kg/m^3]
Silica gel specific heat capacity	921 [J/kg K]
Channel hydraulic diameter	1.5 [mm]
Channel height	1.9 [mm]
Channel width	3.8 [mm]
Channel wall thickness	0.2 [mm]

[a)] Valid for inlet air conditions: 20 °C/60%RH.
[b)] Volumetric air flow rate for density 1.2 kg/m^3.

2.2. Case studies

In the present work, 24 experimental case studies were carried out. The input variables used were the inlet process air humidity ratio, ω_{pi}, the outlet process air flow rate, $\dot{V}_{po}$, the outlet regeneration air flow rate, $\dot{V}_{ro}$, the rotation speed of the DW, R, and the volumetric air flow rate ratio, $\dot{V}_{po}/\dot{V}_{ro}$, see Table 2. The inlet process air temperature, T_{pi}, the inlet regeneration air temperature, T_{ri}, and the inlet regeneration air humidity ratio, ω_{ri}, were fixed at constant values. The combination of the input variables for this study are summarized in Table 3.

2.3. Performance indexes of a desiccant wheel activated at low temperatures

A detailed performance analysis along the entire section of the DW activated at low temperature was carried out. Experimental results of this analysis were evaluated in terms of variation of air humidity ratio, Δω, variation of air temperature, ΔT, for the process air flow and the regeneration air flow, regeneration efficiency, ε_r, and moisture removal

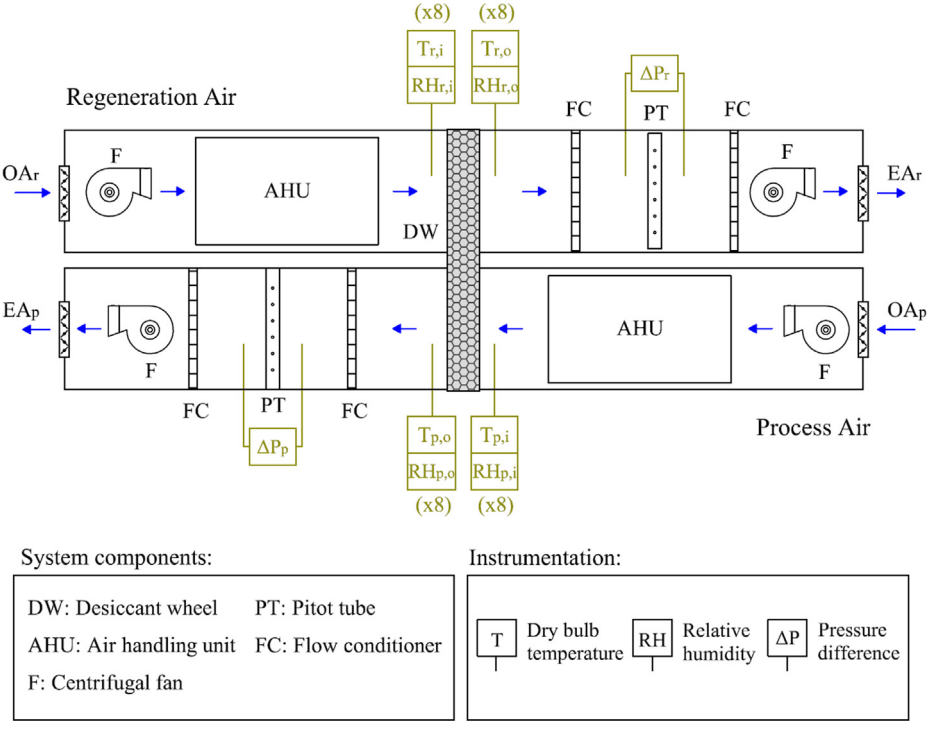

Fig. 1. Layout of the test facility of the desiccant wheel.

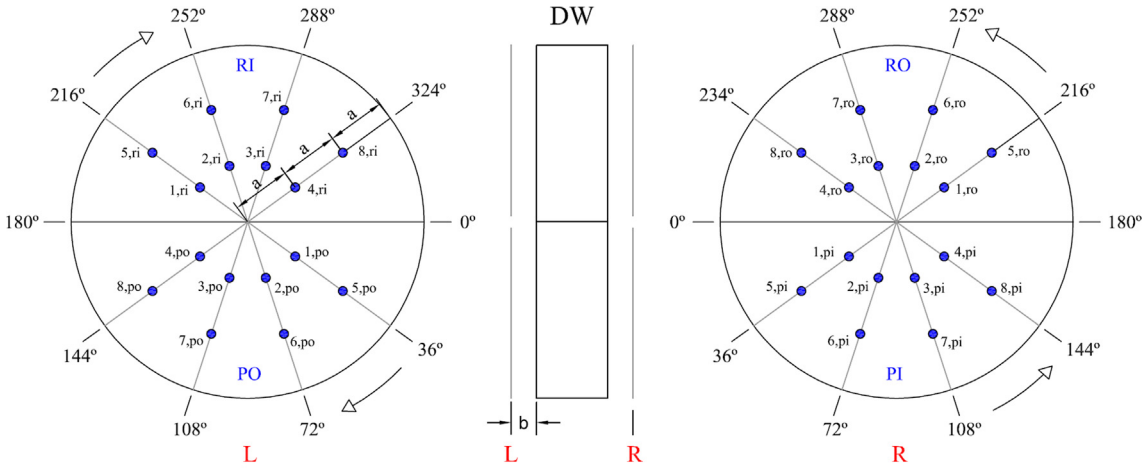

- Sensor of air temperature and relative humidity

Dimensions: a= 91.6 mm; b= 30 mm

Sides: PI: inlet air process; RI: inlet air regeneration

PO: outlet air process; RO: outlet air regeneration

Fig. 2. Distribution of air temperature and humidity sensors on the process and regeneration sides of the DW.

Table 2
Experimental conditions for the case studies.

Variable	Value	Unit
Inlet process air temperature (T_{pi})	30	[°C]
Inlet process air humidity ratio (ω_{pi})	12, 17	[g/kg]
Inlet regeneration air temperature (T_{ri})	45	[°C]
Inlet regeneration air humidity ratio (ω_{ri})	10	[g/kg]
Outlet process air flow rate ($\dot{V}_{po}$)	1000, 1500	[m^3/h]
Outlet regeneration air flow rate ($\dot{V}_{ro}$)	1000, 1500	[m^3/h]
Rotation speed (R)	10, 20, 30, 40	[rph]
Air flow ratio ($\dot{V}_{po}/\dot{V}_{ro}$)	1000/1000, 1000/1500, 1500/1500	[-]

Table 3
Summary of experimental test conditions.

Test	T_{pi} [°C]	ω_{pi} [g/kg]	T_{ri} [°C]	ω_{ri} [g/kg]	$\dot{V}_{po}$[m^3/h]	$\dot{V}_{ro}$[m^3/h]	R [rph]
N1	30	17	45	10	1500	1500	40
N2	30	17	45	10	1500	1500	30
N3	30	17	45	10	1500	1500	20
N4	30	17	45	10	1500	1500	10
N5	30	17	45	10	1000	1500	40
N6	30	17	45	10	1000	1500	30
N7	30	17	45	10	1000	1500	20
N8	30	17	45	10	1000	1500	10
N9	30	17	45	10	1000	1000	40
N10	30	17	45	10	1000	1000	30
N11	30	17	45	10	1000	1000	20
N12	30	17	45	10	1000	1000	10
N13	30	12	45	10	1000	1000	40
N14	30	12	45	10	1000	1000	30
N15	30	12	45	10	1000	1000	20
N16	30	12	45	10	1000	1000	10
N17	30	12	45	10	1000	1500	40
N18	30	12	45	10	1000	1500	30
N19	30	12	45	10	1000	1500	20
N20	30	12	45	10	1000	1500	10
N21	30	12	45	10	1500	1500	40
N22	30	12	45	10	1500	1500	30
N23	30	12	45	10	1500	1500	20
N24	30	12	45	10	1500	1500	10

capacity, MRC. These parameters are defined through the following equations:

- Variation of air humidity ratio, Δω, between the outlet and inlet air.

$$\Delta\omega = \omega_o - \omega_i \tag{1}$$

- Variation of air temperature, ΔT, between the outlet and inlet air.

$$\Delta T = T_o - T_i \tag{2}$$

- Regeneration efficiency, ε_r, represents the ratio of latent energy of the process air achieved with the DW and sensible energy deliverd to thermally activate the DW.

$$\varepsilon_r = \frac{\dot{m}_{po}\cdot(\omega_{pi} - \omega_{po})\cdot\Delta h_{vap}}{\dot{m}_{ro}\cdot(h_{ri} - h_{HC,i})} \tag{3}$$

Where $h_{HC,i}$ is the inlet air enthalpy to the heating coil, which is a constant value (at 25 °C and 50% RH), and Δh_{vap} is the enthalpy of vaporization of water, expressed by Eq. (4), [29].

$$\Delta h_{vap} = -0.614342\cdot10^{-4}\cdot T_{p,i}^3 + 0.158927\cdot10^{-2}\cdot T_{p,i}^2 - 0.236418\cdot10\cdot T_{p,i} + 0.250079\cdot10^4 \tag{4}$$

- Moisture removal capacity, MRC, represents the mass flow rate of moisture removed in the process air by the DW [30].

$$MRC = \dot{m}_{po}\cdot(\omega_{pi} - \omega_{po}) \tag{5}$$

3. Results

3.1. Effect of input variables on the variation of air humidity and temperature of the desiccant wheel

In order to find the relationships between input variables and the variation of air humidity ratio, Δω, and the variation of air temperature, ΔT, of the DW, a detailed analysis for the case study N1, see Table 3, was carried out. Δω and ΔT were calculated by Eqs. (1) and (2). The values of Δω and ΔT for each position of the process and regeneration side of the DW, see Fig. 2, are shown in Fig. 3. Two

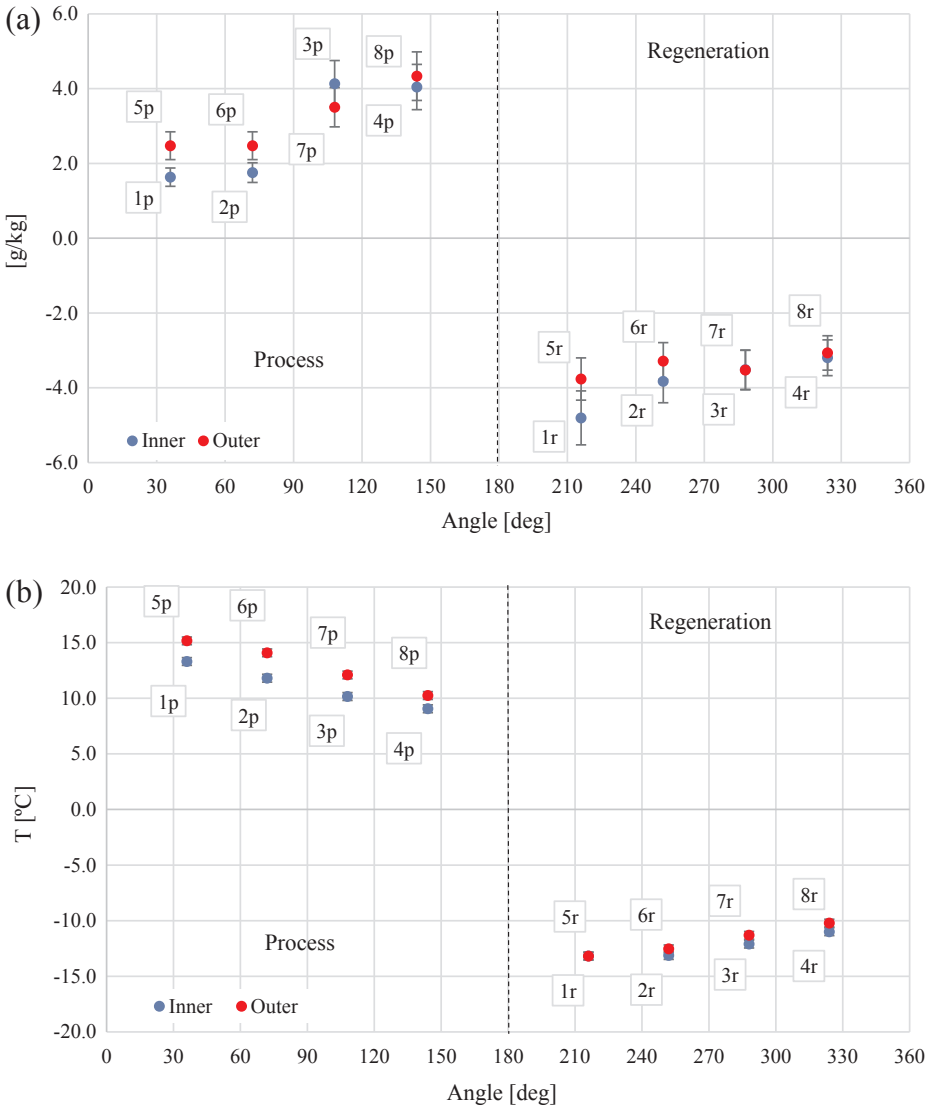

Fig. 3. (a) Δω and (b) ΔT throughout the section of the desiccant wheel.

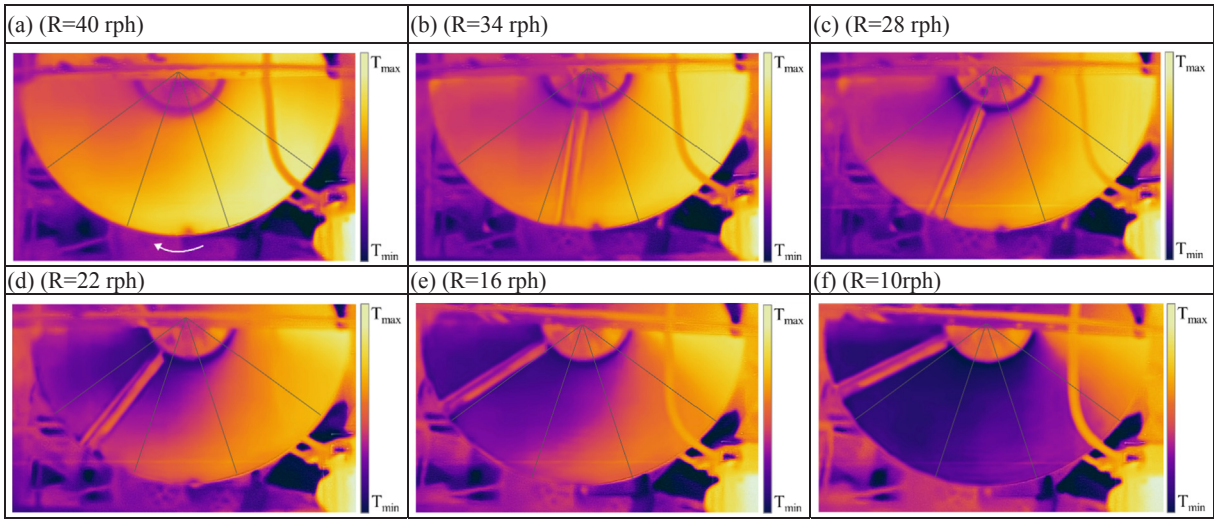

Fig. 4. Thermographic images of the output process side when the rotation speed was varied from 40 rph to 10 rph.

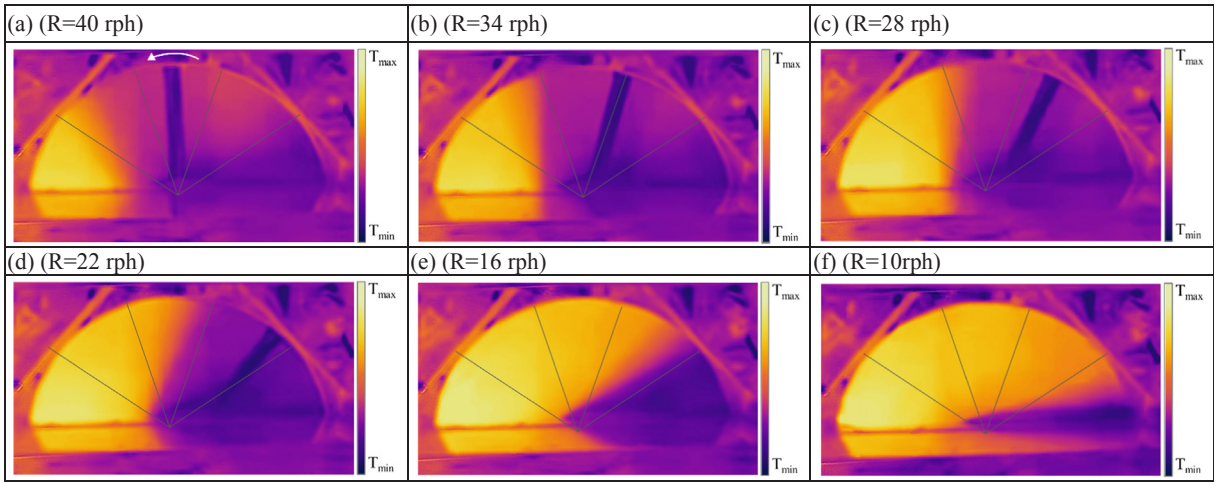

Fig. 5. Thermographic images of the output regeneration side when the rotation speed was varied from 40 rph to 10 rph.

thermographic images of the DW for this case study are shown in Fig. 4a for the process side and in Fig. 5a for the regeneration side.

In the rotation angle of 36° of the process side, air states 1p and 5p in Fig. 3, the results showed an air dehumidification of 2.5 g/kg on the outer radius and 1.6 g/kg on the inner radius, and an air temperature increase of 15.2 °C on the outer radius and 13.3 °C on the inner radius. The dehumidification reached from 0° to 36° was mainly caused by the difference in water vapor pressure between the air and the desiccant material, achieving an adsorption process. The desiccant material in this section was dry, after the regeneration process, so the water vapor pressure in the desiccant material could be lower than that of the air. In this process, the water molecules moved from the moist air to the desiccant due to the differences in water vapor pressure [31]. The desiccant material achieved its maximum process temperature in this circular sector of the DW, as shown in Fig. 4a.

At the angle of 72°, air states 2p and 6p in Fig. 3, the Δω values were similar to those of the previous angles, 2.5 g/kg on the outer radius and 1.8 g/kg on the inner radius. However, the ΔT values for this angle continued to decrease to 14.1 °C on the outer radius and 11.8 °C on the inner radius. This reduction in ΔT was due to the thermal exchange between the air flow and the desiccant material.

At the angle of 108°, air states 3p and 7p in Fig. 3, the Δω values increased to 3.5 g/kg on the outer radius and 4.1 g/kg on the inner radius. A significant reduction in ΔT was obtained for this circular sector of the DW, with a value of 12.1 °C on the outer radius and 10.2 °C on the inner radius, thus being able to reduce the water vapor pressure in the desiccant material. This reduction in ΔT caused greater dehumidification than in previous circular sectors.

At the angle of 144°, air states 4p and 8p in Fig. 3, the Δω values were 4.3 g/kg on the outer radius and 4 g/kg on the inner radius, and the ΔT values were 10.2 °C on the outer radius and 9.1 °C on the inner radius. As the DW turned towards the regeneration side, the desiccant material could adsorb moisture until it reached its maximum dehumidification capacity and thus increased the water vapor pressure on the surface [31]. In the inner radius of the DW, the Δω value of the air state 4p was similar to that of the air state 3p, so the water vapor pressure in the desiccant material at 144° could increase and its adsorption capacity be reduced. However, there was an increase of Δω on the outer radius, so its adsorption capacity increased.

The experimental results of this case study showed that the optimal process air conditions were obtained between 90° and 180°, where the maximum variation of process air humidity ratio and the minimum variation of air temperature and desiccant material temperature both on the inner and outer radius were reached, see Fig. 3 and Fig. 4a.

As the DW turned towards the regeneration side, the regeneration air flow heated the material, see Fig. 5a, and its water vapor pressure increased, allowing the desiccant to release its moisture, and achieving a water desorption process. In contrast to the process side, in the regeneration side, the water molecules moved from the desiccant material to the air flow in order to equalize the differences in water vapor pressure [31]. At an angle of 216°, the Δω values in the air states 1r and 5r were −4.8 g/kg and −3.8 g/kg, respectively, and the ΔT values equal to 13.2 °C in both air states. The minimum temperature of the desiccant material on the regeneration side was obtained in the first circular sector of the DW, between 180° and 216° and the maximum temperature in the last circular sector, between 324° and 360°, see Fig. 3b and Fig. 5a. In this last regeneration circular sector, the desiccant material could have few water molecules on the dry surface, so the water vapor pressure in the desiccant material could be reduced.

The values of Δω and ΔT were usually different at the inner and outer radius for the same rotation angles. The desiccant material reached slightly higher temperature at the outer points that at the inner points. Therefore, the differences of ΔT were mainly due to the desiccant material temperature, see Fig. 4a and Fig. 5a. These differences of ΔT were greater on the process side, approximately 2 °C, see Fig. 3b. The experimental uncertainty of each monitored variable is also shown in Fig. 3.The Δω uncertainty values of the inner radius were usually within the Δω uncertainty values of the outer radius for the same rotation angles. Therefore, the Δω differences between the inner and outer radius for the same rotation angles was not always guaranteed. The ΔT uncertainty values of the inner radius were only within those of the outer radius when the measured ΔT values were equal or very close between both radius, such as air states from 1r to 8 r, see Fig. 3b.

Previous research studies analysed the outlet process air temperature and humidity ratio in the process section of a DW. Nia et al. simulated with a mathematical model the outlet process air humidity ratio for different rotation angles for a case study [19]. The trend of outlet process air humidity ratio was similar to that obtained in Fig. 3a. Yamaguchi and Saito experimentally obtained the outlet process air temperature and humidity ratio in the wheel circumferential and radius directions for another case study, when the DW was activated at high temperature, 80 °C [22]. The trends of process air humidity ratio and temperature were also similar to those obtained in the present work. The previous work also showed that the values of process air humidity ratio and temperature were similar for the inner and outer radius of the DW. However, the temperature values for different radius in a DW activated at low temperature were found to be different in the present work, as shown in Fig. 3. Kang et al. [17] also numerically predicted trends of process air humidity and temperature similar to those obtained by [22].

3.2. Effect of the rotation speed

The effect of the rotation speed, R, of the DW on the parameters $\Delta\omega_p$ and ΔT_p is analysed in the following paragraphs. The inlet air conditions of the process air flow and the regeneration air flow were fixed and the rotation speed was varied to carry out this analysis (tests N1-N4 of Table 3).

The results of $\Delta\omega_p$ and ΔT_p for each air state and for different R values are shown in Fig. 6. The trends of $\Delta\omega_p$ and ΔT_p for the four cases studied were similar to those analysed in Fig. 3. It can be observed than the first air states of the process side, states 1p and 5p, achieved similar ΔT_p values, regardless of the R value. Similar $\Delta\omega_p$ values were also obtained for R equal to 30 rph (test N2), 20 rph (test N3) and 10 rph (test N4). However, for a R value equal to 40 rph (test N1), the $\Delta\omega_p$ value increased slightly compared to the other R values. The $\Delta\omega_p$ values remained constant for all rotation speeds from air state 5p to 6p and from air state 1p to 2p, because the differences in water vapor pressure between the air and the desiccant material could be similar. However, the ΔT_p values decreased from air state 5p to 6p and from air state 1p to 2p.

For the air states 3p and 7p, rotation angle 108°, the values of $\Delta\omega_p$ increased significantly and the values of ΔT_p decreased. The highest value of $\Delta\omega_p$ in the inner radius was obtained in the air state 3p. However, the highest value of $\Delta\omega_p$ in the outer radius were achieved in the air state 8p. The $\Delta\omega_p$ values in 3p and 8p were quite similar, so this $\Delta\omega_p$ could be the maximum desiccant capacity of the DW for these air conditions.

The qualitative surface temperatures of the desiccant material on the output process side and the output regeneration side when the rotation speed was varied from 40 rph to 10 rph are shown in Fig. 4 and Fig. 5, respectively. For the process side, it can be observed that the temperature of the desiccant material was lower in the last circular sector closer to the regeneration side, see Fig. 4. The lower the R value the lower the mean surface temperature, as shown in Fig. 4. Conversely, for the regeneration side, the lower the R value the higher the mean surface temperature, as shown in Fig. 5. The surface temperatures of the desiccant material on the output process side varied with the angular and radial position, see Fig. 4. However, the surface temperatures of the desiccant material on the output regeneration side varied only with the angular position, see Fig. 5. These temperature changes were in agreement with the air temperature results shown in Fig. 3. The ΔT values of the process side were usually different at the inner and outer radius for the same rotation angles, see Fig. 3a, whereas, the ΔT values of the regeneration side were similar at the inner and outer radius, see Fig. 3b.

The effect of the rotation speed, R, on the regeneration efficiency, ε_r, in each circular sector of the DW was analysed on the process side. The ε_r values throughout this section for the tests N1-N4 are represented in Fig. 7. It can be seen that the area with greater efficiency was obtained in the last circular sector closer to the regeneration side. The higher the rotation speed, the greater the area of this circular sector, as shown in N1, Fig. 7a. For N1, the ε_r values were greater than 0.2 from the rotation angle of 72° to 180°. The maximum ε_r value for N1 was obtained in the air state 8p, see Fig. 2, with a ε_r value equal to 0.52. However, for N4, the ε_r values were greater than 0.2 for the circular sector between 144° and 180°.

The average values of $\Delta\omega_p$, ΔT_p and ε_r for each R value for the tests N1-N4 are shown in Table 4. It can be observed that the highest average values of $\Delta\omega_p$, ΔT_p and ε_r were obtained for N1 and the lowest values for N4. These results suggest that by properly selecting the rotation speed, a larger circular sector of the DW with greater efficiency may be obtained, and consequently greater air dehumidification may be achieved.

3.3. Effect of the air flow rates

The effect of the outlet process and regeneration air flow rates of the DW on the parameters $\Delta\omega_p$ and ΔT_p was also studied in the present work. First, the different air states of the process section were analysed when the DW operated with balanced air flow rates, i.e. the values of $\dot{V}_{po}$ and $\dot{V}_{ro}$ were equal, and then, when it operated with unbalanced air flow rates, i.e. the values of $\dot{V}_{po}$ and $\dot{V}_{ro}$ were different.

3.3.1. Balanced air flow rates

The values of $\Delta\omega_p$ and ΔT_p for each air state for different balanced air flow rates, $\dot{V}_{po}$ and $\dot{V}_{ro}$, and different inlet process air humidity ratio, ω_{pi}, are represented in Fig. 8. The remaining input variables were fixed at constant values. The case studies analysed were N1, N9, N21 and N13, see Table 3.

The ΔT_p values for low air flow rates, such as tests N9 and N13 with 1000 m^3/h, were higher than those obtained for high air flow rates, such as tests N1 and N21 with 1500 m^3/h, so the outlet air temperature of the process stream was higher for low air flow rates.

The $\Delta\omega_p$ values of the first air states, 1p and 5p, for low air flow rates, N9 and N13, were lower than those obtained for high air flow rates, N1 and N21, so the initial desiccant capacity of the DW was lower for low air flow rates. This process was due to the fact that the desiccant material on the regeneration side reached a higher temperature for low air flow rates than for high air flow rates, which could cause an increase in the water vapor pressure of the desiccant material.

It can also be observed than the maximum value of $\Delta\omega_p$ in the inner radius of the DW for N1, with air flow rates equal to 1500 m^3/h, was achieved in the state 3p, as mentioned previously in Section 3.1. This value was slightly reduced in the state 4p, so the material reduced its

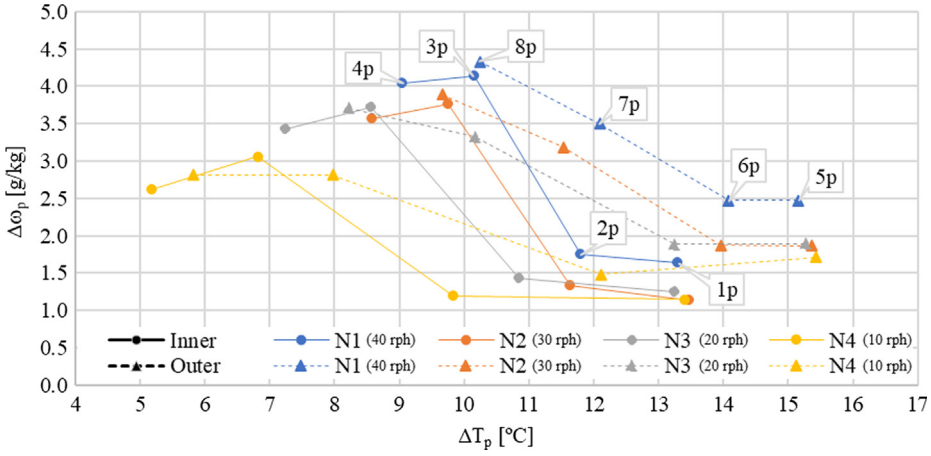

Fig. 6. Relationship of $\Delta\omega_p$ on ΔT_p throughout the process section of the desiccant wheel for different rotation speeds, tests N1-N4.

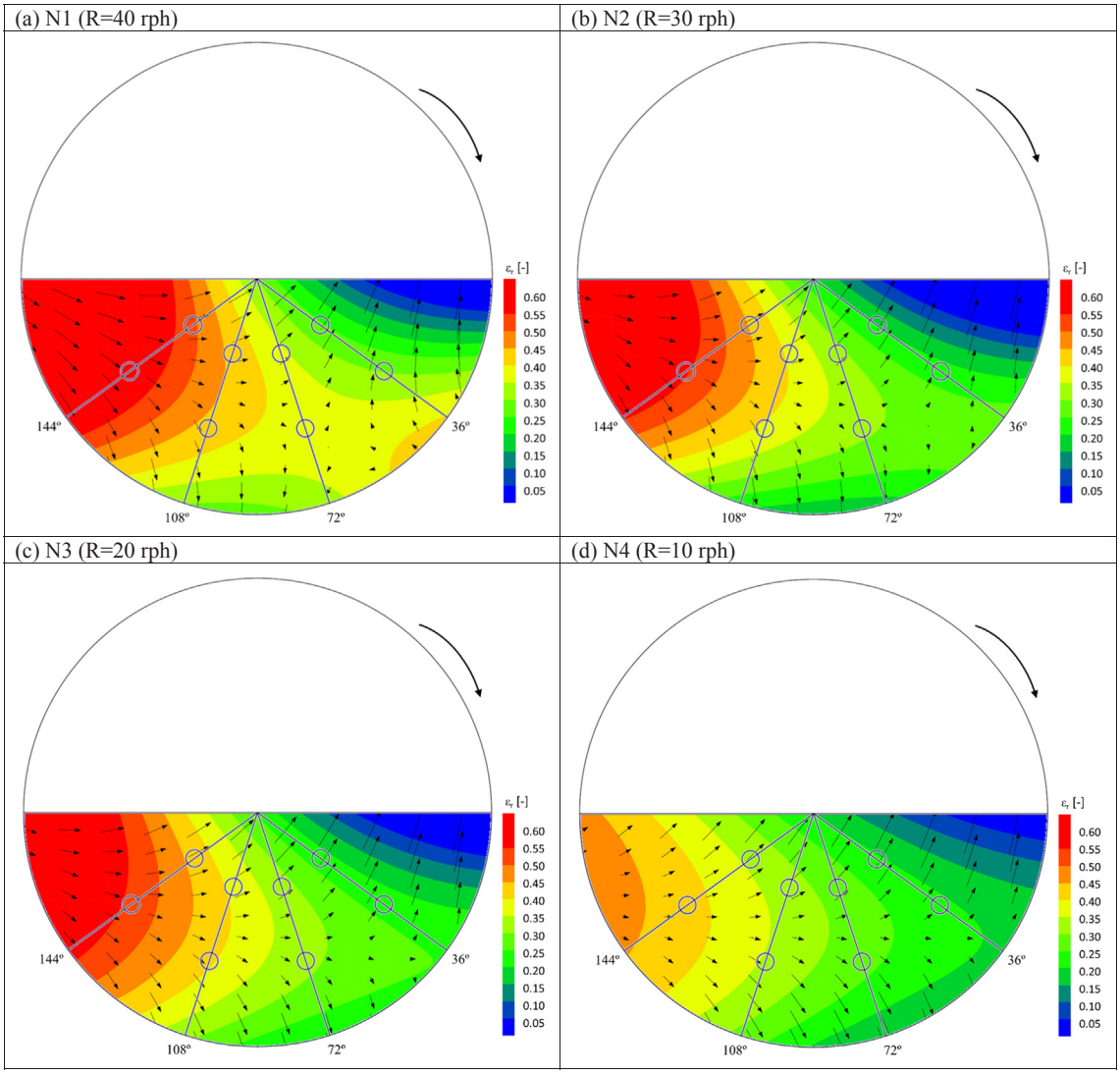

Fig. 7. Contour line plots of ε_r for the tests N1-N4.

Table 4
Average values of $\Delta\omega_p$, ΔT_p and ε_r for the tests N1-N4.

Test	R [rph]	$\overline{\Delta\omega_p}$ [g/kg]	$\overline{\Delta T_p}$ [°C]	$\overline{\varepsilon_r}$ [-]
N1	40	3.0	12.0	0.36
N2	30	2.6	11.7	0.31
N3	20	2.5	10.9	0.30
N4	10	2.1	9.6	0.25

dehumidification capacity. However, for N9, with air flow rates equal to 1000 m^3/h, the maximum value of $\Delta\omega_p$ in the inner radius was achieved in the state 4p.

The variation of the maximum and minimum values of $\Delta\omega_p$ and ΔT_p along the wheel section was greater for high ω_{pi} values, as shown in the air states of N1 compared to those of N21 and, the air states of N9 compared to those of N13, see Fig. 8. For wet air streams, such as case studies N1 and N9 with ω_{pi} equal to 17 g/kg, the water vapor pressure in the air could be higher than for dry air streams, so the difference in water vapor pressure between the air and the desiccant material could be higher for N1 and N9.

3.3.2. Unbalanced air flow rates

Another feasible method of controlling dehumidification capacity can be through the use of unbalanced air flow rates. The profiles of $\Delta\omega_p$ and ΔT_p along the wheel section for unbalanced air flow rates, test N5, was represented in Fig. 9, in order to compare these results with those obtained for the tests N1 and N9 with balanced air flow rates. The remaining input variables were fixed at constant values, as shown in Table 3. The results of N5 showed greater values of $\Delta\omega_p$ and ΔT_p throughout the process section than those of N1, achieving a maximum peak of $\Delta\omega_p$ in 8p, 5.3 g/kg, and a maximum peak of ΔT_p in 5p, 13.6 °C. The air dehumidification for N5 was greater than that for N1, although the latent heat of the inlet process air for N5 was lower than that for N1, since $\dot{V}_{po}$ of N5 was lower than $\dot{V}_{po}$ of N1. The values of $\Delta\omega_p$ and ΔT_p for N9 were also lower than that for N5, because the thermal energy used to regenerate the DW was higher for N5 than for N9, so there was a greater desorption of water vapor on the regeneration side.

The ε_r parameter was also obtained throughout the process section of the DW for different air flow rates. The ε_r values on the process side of the DW for the tests N9, N21 and N13, with balanced air flow rates, and the test N5, with unbalanced air flow rates, are shown Fig. 10.

The ε_r results obtained for N9, see Fig. 10a, with balanced air flow rates equal to 1000 m^3/h and ω_{pi} equal to 17 g/kg, were similar to those obtained for N1, with balanced flows equal to 1500 m^3/h and ω_{pi} equal to 17 g/kg, see Fig. 7a. For both case studies, the maximum ε_r value was obtained in the last circular sector of the DW, between 144° and 180°, and the minimum ε_r value in the first circular sector, between 0° and 36°, obtaining great efficiency differences between both circular

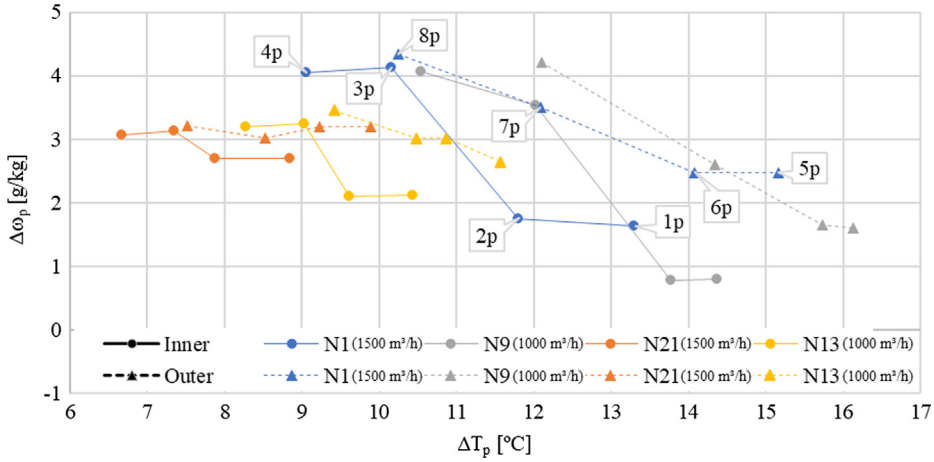

Fig. 8. Relationship of $\Delta\omega_p$ on ΔT_p throughout the process section of the desiccant wheel for different balanced air flow rates and humidity ratio, tests N1, N9, N21 and N13.

sectors. However, for the tests N21 and N13, with balanced air flow rates and ω_{pi} equal to 12 g/kg, the variation in ε_r between the different circular sectors was smaller than in N1 and N9, i.e. the ε_r values were similar throughout the process section, between 0° and 180°, see Fig. 10b and Fig. 10c.

For the test N5, see Fig. 10d, with unbalanced air flow rates and ω_{pi} equal to 17 g/kg, the trend of the ε_r values was similar to that of N1 and N9, see Fig. 7a and Fig. 10a. A maximum ε_r peak was obtained in the air state 8p, with ε_r equal to 0.48, coinciding with the circular sector of the DW with the highest air dehumidification, between 108° and 180°, see Fig. 9.

The average values of $\Delta\omega_p$, ΔT_p and ε_r for the tests N9, N21, N13 and N5 are shown in Table 5. It can be observed than the $\overline{\Delta\omega_p}$ values for high and balanced air flow rates, such as N1, Table 4, and N21, Table 5, were higher than those for low and balanced air flow rates, such as N9 and N13. Moreover, the $\overline{\Delta T_p}$ values for high and balanced air flow rates were lower than those for low and balanced air flow rates, when ω_{pi} was fixed at a constant value, because the temperature of the desiccant material was higher for low and balanced air flow rates. The average values of ε_r for N1 and N21 with high and balanced air flow rates were also slightly higher than those for N9 and N13 with low and balanced air flow rates. Regarding $\overline{\varepsilon_r}$ for different ω_{pi}, the maximum ε_r values for N21 and N13, with ω_{pi} equal to 12 g/kg, were lower than those for N1 and N9, with ω_{pi} equal to 17 g/kg, as shown in Fig. 7 and Fig. 10. However, $\overline{\varepsilon_r}$ was similar for different ω_{pi} when the air flow rates were fixed at constant values, see Table 5.

For the test N5, with unbalanced air flow rates and ω_{pi} equal to 17 g/kg, the average air dehumidification, $\overline{\Delta\omega_p}$, was higher than that for N9, with balanced air flow rates and ω_{pi} equal to 17 g/kg, see Table 5, because the regeneration energy used in N5 was greater than that in N4, through a higher regeneration air flow rate. $\overline{\Delta T_p}$ for N5 was also higher than for N9, so the outlet process air temperature was higher. However, the $\overline{\varepsilon_r}$ values were the same for both case studies. The unbalanced air flow rates allow a greater range of adjustment on the outlet air humidity ratio, but with a higher outlet air temperature.

3.4. Analysis of overall moisture removal capacity of the DW

The overall moisture removal capacity, MRC, of the DW was analysed for all cases studied, N1-N24, see Table 3. The results of $\overline{MRC}$, $\overline{\Delta\omega_p}$ and $\overline{\Delta T_p}$ are shown in Table 6. It can be observed that the same $\overline{MRC}$ value can be obtained by controlling the air flow rates or the rotation speed.

- For N2 and N6, $\overline{MRC}$ was equal to 4.7 kg/h modifying $\dot{V}_{po}$ from 1500 m^3/h to 1000 m^3/h.
- For N5 and N8, $\overline{MRC}$ was equal to 4.3 kg/h modifying R from 40 rph to 10 rph, or for N11 varying $\dot{V}_{ro}$ from 1500 m^3/h to 1000 m^3/h.
- For N13 and N15, $\overline{MRC}$ was equal to 3.4 kg/h modifying R from 40 rph to 20 rph, and further, for N24 modifying $\dot{V}_{po}$ and $\dot{V}_{ro}$ from 1000 m^3/h to 1500 m^3/h.

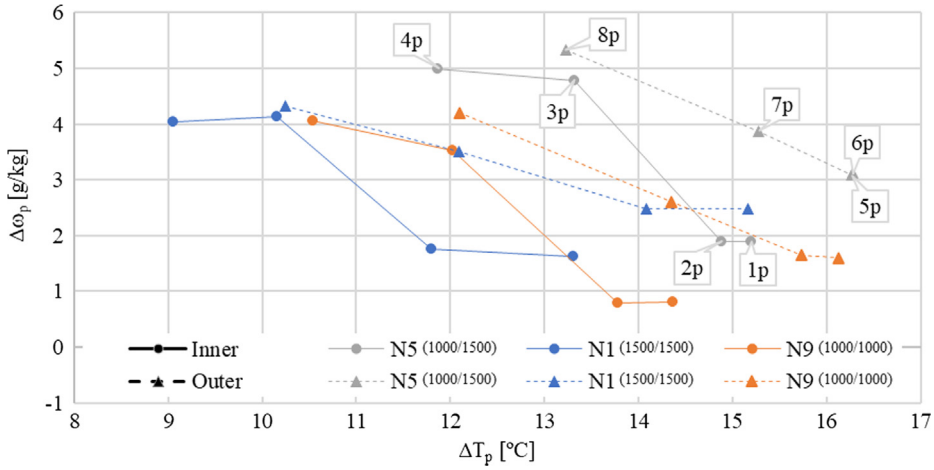

Fig. 9. Relationship of $\Delta\omega_p$ on ΔT_p throughout the process section of the DW for unbalanced air flow rates, test N5, and unbalanced air flow rates, tests N1 and N9.

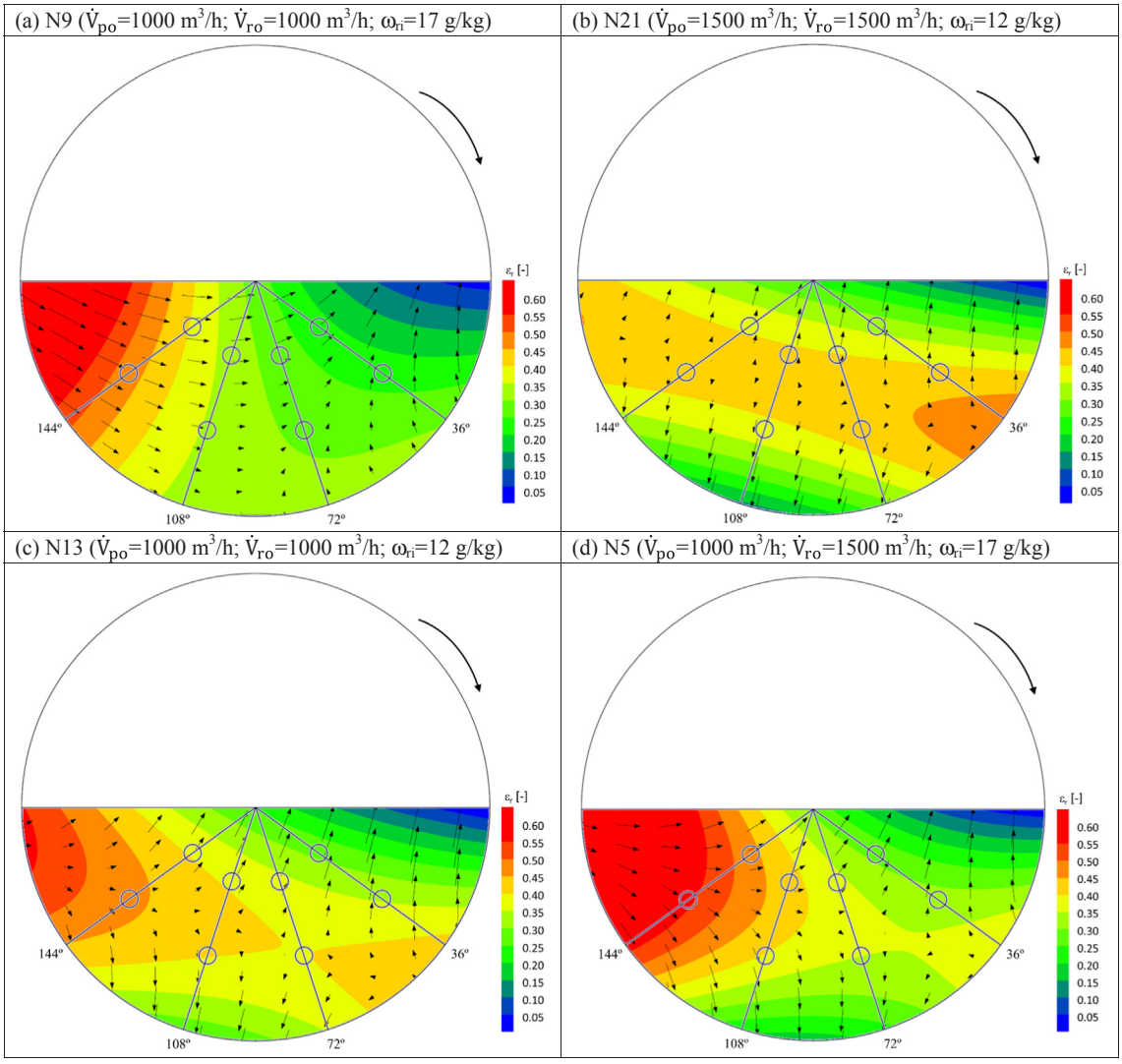

Fig. 10. Contour line plots of ε_r for the tests N9, N21, N13 and N5.

Table 5
Average values of $\Delta\omega_p$, ΔT_p and ε_r for the tests N9, N21, N13 and N5.

Test	$\dot{V}_{po}/\dot{V}_{ro}$	ω_{pi} [g/kg]	$\overline{\Delta\omega_p}$ [g/kg]	$\overline{\Delta T_p}$ [°C]	$\overline{\varepsilon_r}$ [-]
N9	1000/1000	17	2.4	13.6	0.34
N21	1500/1500	12	3.0	8.2	0.35
N13	1000/1000	12	2.8	10	0.33
N5	1000/1500	17	3.6	14.5	0.34

For all three cases, the same value of $\overline{MRC}$ was obtained, but with different values of $\overline{\Delta T_p}$, i.e. there was the same mass transfer in the DW, but different heat transfer. In addition, the energy consumption of the fans varied when the process and regeneration air flow rates were modified, therefore, greater energy savings can be achieved with a suitable control strategy. These results show that the wheel control strategy can be designed so that the dehumidification capacity is greater, and the sensible thermal energy is lower, improving the DW efficiency. Previous research studies showed that a control strategy for DW activated at low temperatures, would allow MRC, T_{po} and ω_{po} to be controlled by setting the process airflow rate and air regeneration temperature [2]. Other studies on DW also analysed the effects of different inlet air conditions and rotation speed on MRC [14,32]. The results showed dehumidification trends similar to those obtained in the present work.

Table 6
Results of experimental test conditions.

Test	$\overline{\Delta\omega_p}$ [g/kg]	$\overline{\Delta T_p}$ [°C]	$\overline{MRC}$ [kg/h]	Test	$\overline{\Delta\omega_p}$ [g/kg]	$\overline{\Delta T_p}$ [°C]	$\overline{MRC}$ [kg/h]
N1	3.0	12.0	5.4	N13	2.8	10	3.4
N2	2.6	11.7	4.7	N14	3.2	9.8	3.8
N3	2.5	10.9	4.5	N15	2.8	9.7	3.4
N4	2.1	9.6	3.8	N16	2.7	8.4	3.2
N5	3.6	14.5	4.3	N17	4.0	12	4.8
N6	3.9	13.9	4.7	N18	3.9	11.6	4.7
N7	3.8	13.8	4.6	N19	3.8	10.8	4.6
N8	3.6	12.0	4.3	N20	3.0	8.8	3.6
N9	2.4	13.6	2.9	N21	3.0	8.2	5.4
N10	3.3	11.9	4.0	N22	2.9	8.3	5.2
N11	3.6	11.4	4.3	N23	2.4	8.7	4.3
N12	3.5	10.9	4.2	N24	1.9	7.7	3.4

4. Conclusions

In the present work the performance of different circular sectors of a DW activated at low temperatures under different working conditions was determined experimentally. In the case studies carried out, the DW performance was studied for different rotation speeds and different process and regeneration air flow rates. The air temperature and humidity were measured in 32 different locations and a thermographic

camera was also used to obtain thermal images of the desiccant material surface.

The experimental results showed that the maximum temperatures of the outlet process air and process desiccant material were obtained in the first circular sector of the DW, between 0° and 36°, and the minimum temperatures in the last circular sector, between 144° and 180°. On the contrary, for the regeneration side, the maximum temperatures of the outlet air and desiccant material were obtained in the last circular sector of the DW, between 234° and 0°, and the minimum temperatures in the first circular sector, between 180° and 216°. These differences of the desiccant material temperature caused differences of outlet air humidity ratio throughout the section of the DW. The maximum air dehumidification was achieved in the last process circular sector of the DW and the minimum in the first process circular sector. Moreover, the values of the outlet air temperature and humidity ratio were usually different in the inner and outer radius of the DW for the same rotation angles.

The results of the case studies analysed showed that the lower the rotation speed, the lower the surface temperatures of the desiccant material on the process side. On the contrary, the lower the rotation speed, the higher the surface temperatures of the desiccant material on the regeneration side.

The regeneration efficiency throughout the process section of the DW showed that the highest efficiency values were obtained in the last circular sector closer to the regeneration side. The number of circular sectors where the highest efficiency values were obtained increased when the rotation speed or air flow rates increased.

Similar values of average moisture removal capacity of the DW were obtained for several case studies with different rotation speeds and air flow rates. However, for these case studies, different outlet process air temperatures were obtained. Therefore, these results suggest that a suitable control strategy can be designed so that the dehumidification capacity is greater, and the sensible thermal energy is lower, improving the DW efficiency.

These experimental results strengthen the performance analysis of desiccant wheels activated at low temperatures, as well as their use as an interesting alternative to conventional dehumidification systems.

Declaration of Competing Interest

The authors declare that they have no known competing financial interests or personal relationships that could have appeared to influence the work reported in this paper.

Acknowledgement

The authors acknowledge the financial support received by the European Regional Development Fund and the Andalusian Economy, Knowledge, Enterprise and University Council, Spain, through the research project HICOOL, reference 1263034, and by European Union's Horizon 2020 research and innovation programme, through the research project WEDISTRICT, reference H2020-WIDESPREAD2018-03-857801.

References

[1] European Parliament, European Directive 2010/31/EU on the Energy Performance of Buildings, 2010. http://doi.org/10.3000/17252555.L_2010.153.eng.
[2] F. Comino, M. Ruiz de Adana, Experimental and numerical analysis of desiccant wheels activated at low temperatures, Energy Build. 133 (2016), https://doi.org/10.1016/j.enbuild.2016.10.021.
[3] J. Wrobel, P. Morgenstern, G. Schmitz, Modeling and experimental validation of the desiccant wheel in a hybrid desiccant air conditioning system, Appl. Therm. Eng. 51 (2013) 1082–1091, https://doi.org/10.1016/j.applthermaleng.2012.09.033.
[4] F. Comino, M. Ruiz de Adana, F. Peci, Energy saving potential of a hybrid HVAC system with a desiccant wheel activated at low temperatures and an indirect evaporative cooler in handling air in buildings with high latent loads, Appl. Therm. Eng. 131 (2018) 412–427, https://doi.org/10.1016/j.applthermaleng.2017.12.004.
[5] D. Pandelidis, A. Pacak, A. Cichoń, S. Anisimov, P. Drąg, B. Vager, V. Vasilijev, Multi-stage desiccant cooling system for moderate climate, Energy Convers. Manag. 177 (2018) 77–90, https://doi.org/10.1016/j.enconman.2018.09.061.
[6] C. Roselli, M. Sasso, F. Tariello, Assessment of a solar PV-driven desiccant-based air handling unit with different tracking systems, Sustain. Energy Technol. Assessments. 34 (2019) 146–156, https://doi.org/10.1016/j.seta.2019.04.013.
[7] D. Pandelidis, S. Anisimov, W.M. Worek, P. Drag, Comparison of desiccant air conditioning systems with different indirect evaporative air coolers, Energy Convers. Manag. 117 (2016) 375–392, https://doi.org/10.1016/j.enconman.2016.02.085.
[8] C.H. Chen, C.Y. Hsu, C.C. Chen, Y.C. Chiang, S.L. Chen, Silica gel/polymer composite desiccant wheel combined with heat pump for air-conditioning systems, Energy. 94 (2016) 87–99, https://doi.org/10.1016/j.energy.2015.10.139.
[9] F. Comino, J. Castillo González, F.J. Navas-Martos, M. Ruiz de Adana, Experimental energy performance assessment of a solar desiccant cooling system in Southern Europe climates, Appl. Therm. Eng. 165 (2020) 114579. http://doi.org/10.1016/j.applthermaleng.2019.114579.
[10] P. Bareschino, F. Pepe, C. Roselli, M. Sasso, F. Tariello, Desiccant-Based Air Handling Unit Alternatively Equipped with Three Hygroscopic Materials and Driven by, Solar Energy (2019).
[11] Y. Guan, Y. Zhang, Y. Sheng, X. Kong, S. Du, Feasibility and economic analysis of solid desiccant wheel used for dehumidification and preheating in blast furnace: A case study of steel plant, Nanjing, China, Appl. Therm. Eng. 81 (2015) 426–435, https://doi.org/10.1016/j.applthermaleng.2015.02.006.
[12] F. Comino, D. Guijo-Rubio, M. Ruiz de Adana, C. Hervás-Martínez, Validation of multitask artificial neural networks to model desiccant wheels activated at low temperature, Int. J. Refrig. 100 (2019), https://doi.org/10.1016/j.ijrefrig.2019.02.002.
[13] X.N. Wu, T.S. Ge, Y.J. Dai, R.Z. Wang, Review on substrate of solid desiccant dehumidification system, Renew. Sustain. Energy Rev. 82 (2018) 3236–3249, https://doi.org/10.1016/j.rser.2017.10.021.
[14] J.D. Chung, Modeling and Analysis of Desiccant Wheel. In: Enteria N., Awbi H., Yoshino H. (eds) Desiccant Heating, Ventilating, and Air-Conditioning Systems, 2016. http://doi.org/10.1007/978-981-10-3047-5.
[15] P. Stabat, D. Marchio, Heat and mass transfer modeling in rotary desiccant dehumidifiers, Appl. Energy. 86 (2009) 762–771, https://doi.org/10.1016/j.apenergy.2007.06.018.
[16] S. De Antonellis, C.M. Joppolo, L. Molinaroli, Simulation, performance analysis and optimization of desiccant wheels, Energy Build. 42 (2010) 1386–1393, https://doi.org/10.1016/j.enbuild.2010.03.007.
[17] H. Kang, S. Choi, D.Y. Lee, Analytic solution to predict the outlet air states of a desiccant wheel with an arbitrary split ratio, Energy. 153 (2018) 301–310, https://doi.org/10.1016/j.energy.2018.03.177.
[18] H. Kang, G. Lee, D.Y. Lee, Explicit analytic solution for heat and mass transfer in a desiccant wheel using a simplified model, Energy. 93 (2015) 2559–2567, https://doi.org/10.1016/j.energy.2015.10.091.
[19] F.E. Nia, D. van Paassen, M.H. Saidi, Modeling and simulation of desiccant wheel for air conditioning, Energy Build. 38 (2006) 1230–1239, https://doi.org/10.1016/j.enbuild.2006.03.020.
[20] P. Bareschino, G. Diglio, F. Pepe, G. Angrisani, C. Roselli, M. Sasso, Modelling of a rotary desiccant wheel: Numerical validation of a Variable Properties Model, Appl. Therm. Eng. 78 (2015) 640–648, https://doi.org/10.1016/j.applthermaleng.2014.11.063.
[21] M. Ali, V. Vukovic, M.H. Sahir, D. Basciotti, Development and validation of a desiccant wheel model calibrated under transient operating conditions, Appl. Therm. Eng. 61 (2013) 469–480, https://doi.org/10.1016/j.applthermaleng.2013.08.010.
[22] S. Yamaguchi, K. Saito, Numerical and experimental performance analysis of rotary desiccant wheels, Int. J. Heat Mass Transf. 60 (2013) 51–60, https://doi.org/10.1016/j.ijheatmasstransfer.2012.12.036.
[23] N. Enteria, H. Yoshino, A. Satake, A. Mochida, R. Takaki, R. Yoshie, T. Mitamura, S. Baba, Experimental heat and mass transfer of the separated and coupled rotating desiccant wheel and heat wheel, Exp. Therm. Fluid Sci. 34 (2010) 603–615, https://doi.org/10.1016/j.expthermflusci.2009.12.001.
[24] U. Eicker, U. Schürger, M. Köhler, T. Ge, Y. Dai, H. Li, R. Wang, Experimental investigations on desiccant wheels, Appl. Therm. Eng. 42 (2012) 71–80, https://doi.org/10.1016/j.applthermaleng.2012.03.005.
[25] L.Z. Zhang, H.X. Fu, Q.R. Yang, J.C. Xu, Performance comparisons of honeycomb-type adsorbent beds (wheels) for air dehumidification with various desiccant wall materials, Energy. 65 (2014) 430–440, https://doi.org/10.1016/j.energy.2013.11.042.
[26] H. Kang, D.Y. Lee, Experimental investigation and introduction of a similarity parameter for characterizing the heat and mass transfer in polymer desiccant wheels, Energy. 120 (2017) 705–717, https://doi.org/10.1016/j.energy.2016.11.122.
[27] T. Higashi, M. Yamaguchi, N. Nakagawa, C. Dang, E. Hihara, Gravimetric method for sorption performance measurement of desiccant wheel and desiccant coated heat exchanger, Appl. Therm. Eng. 144 (2018) 639–646, https://doi.org/10.1016/j.applthermaleng.2018.05.079.
[28] F. Comino, M. Ruiz de Adana, F. Peci, First and second order simplified models for the performance evaluation of low temperature activated desiccant wheels, Energy Build. 116 (2016) 574–582, https://doi.org/10.1016/j.enbuild.2016.02.005.
[29] G. Angrisani, F. Minichiello, C. Roselli, M. Sasso, Experimental analysis on the dehumidification and thermal performance of a desiccant wheel, Appl. Energy. 92 (2012) 563–572, https://doi.org/10.1016/j.apenergy.2011.11.071.
[30] ASHRAE, Method of testing for rating desiccant dehumidifiers utilizing heat for the regeneration process, ASHRAE standard, 2007.

[31] C. Zhai, D.H. Archer, J.C. Fischer, Performance modeling of desiccant wheels (1): Model development, in: 2008 Proc. 2nd Int. Conf. Energy Sustain. ES 2008, 2009. http://doi.org/10.1115/es2008-54185.

[32] A. Al-Alili, Y. Hwang, R. Radermacher, Performance of a desiccant wheel cycle utilizing new zeolite material: Experimental investigation, Energy. 81 (2015) 137–145, https://doi.org/10.1016/j.energy.2014.11.084.